Struct Multidisc Optim (2008) 35:523–530
DOI 10.1007/s00158-007-0126-2

RESEARCH PAPER

Probabilistic optimal design in the presence of random fields

Samy Missoum

Received: 17 October 2006 / Revised: 6 January 2007 / Accepted: 23 February 2007 / Published online: 2 June 2007

Abstract This article describes a methodology to incorporate a random field in a probabilistic optimization problem. The approach is based on the extraction of the features of a random field using a reduced number of experimental observations. This is achieved by proper orthogonal decomposition. Using Lagrange interpolation, a modified random field is obtained by changing the contribution of each feature. The contributions are controlled using scalar parameters, which can be considered as random variables. This allows one to perform a random-field-based probabilistic optimization with few random variables. The methodology is demonstrated on a tube impacting a rigid wall for which a random field modifies the planarity of the tube's wall.

Keywords Probabilistic optimal design · Random fields · Proper orthogonal decomposition

1 Introduction

In mechanics, it is well known that spatially varying random fields are often a more realistic representation of uncertainties than space-independent random variables. For instance, the actual thickness distribution of a metal sheet is characterized by a deviation from its nominal desired value. This deviation is not constant over the whole sheet but is function of the position. This notion of field can also be understood by considering spatial variations of material properties such as the Young's modulus.

Accounting for spatial variations of uncertainties is essential in applications such as crashworthiness. For instance, the distribution of residual stresses after metal forming has a marked influence on the crash behavior (Oliveiraa et al. 2006). A position-independent random variable would not accurately represent this situation. In addition, the highly nonlinear behavior exhibits an acute sensitivity to uncertainties (Missoum 2007) and makes it difficult to create a reasonably "conservative" description of uncertainties.

In the probabilistic design literature, many studies quantify uncertainties using random variables. These works are mainly focused on reliability assessment with techniques such as Monte Carlo simulation and first- and second-order reliability methods (Haldar and Mahadevan 2000; Melchers 1999). A large portion of publications is also dedicated to reliability-based design optimization (Adams et al. 2006; Kharmanda et al. 2002; Youn and Choi 2004) and robust design (Trosset et al. 2003).

On the other hand, stochastic finite elements (SFE) have set a rigorous framework to understand and quantify how uncertainties, in the form of random fields, propagate through a model and how the system's responses are affected (Ghanem and Spanos 1991). SFE are based on the notion of polynomial chaos, which expands inputs and responses of a system on a specific polynomial basis.

Manuscript for the Special Issue for the Symposium on Design Optimization Applications in Industry at the Seventh World Congress on Computational Mechanics.

Organizer: Ren-Jye Yang

S. Missoum (✉)
Department of Aerospace and Mechanical Engineering,
The University of Arizona, 1130 N. Mountain,
P.O. Box 210119, Tucson, Arizona 85721, USA
e-mail: smissoum@ame.arizona.edu

One of the restrictions of SFE is that strong assumptions on the probabilistic description of the random field are needed. For instance, a Gaussian random field can be chosen. In a practical situation, such as a random field generated by a manufacturing process, the nature of the random field is not known a priori. Therefore, and this is one of the key elements of this article, the only way to characterize a random field with a certain level of confidence is from experimental observations.

Based on a limited number of observations, the use of proper orthogonal decomposition (POD) allows one to extract the main *features* of a random field in the form of eigenvectors of its correlation matrix. The eigenvalues provide an indication of the "importance" of the corresponding features, thus allowing to gauge their individual contributions to the random field. This paper describes a technique to efficiently extract the features. This technique is not new and originates from image recognition (Turk and Pentland 1991).

Once the main features of the random field are known and ranked by order of importance, this paper presents an approach by which the random field is modified by weighing each feature differently, thus modifying its contribution. By varying these "weights," it is possible to describe many potential random fields. That is, if the weights are considered as random variables, the description of a whole complex random field has been reduced to a handful set of variables. In the context of probabilistic optimization, this simplified and reduced description provides a very powerful tool for a more realistic optimization.

Two application examples are presented. The first one aims at demonstrating the respective influences of two features of a random field on the linear buckling of a plate. The second example deals with the optimization of a tube impacting a rigid wall. A random field modifies the planarity of the tube's sides, thus, changing its highly nonlinear dynamic behavior. The objective of the second problem is to find two positions of structural fuses so as to maximize the probability of having an energy absorption above a given value.

2 Random field and correlation matrix

Consider the output of a process (e.g., a metal sheet after forming). The process generates a scalar random field $S(\mathbf{X})$, function of the position $\mathbf{X}$. m samples, outputs of this process, are obtained. On each sample, n measurements are performed at distinct positions. An example of observations, referred to as snapshots, is provided in Fig. 1. The snapshots can be condensed in the following matrix:

$$\mathbf{S} = \begin{pmatrix} S_{11} & \dots & S_{1m} \\ \vdots & \ddots & \vdots \\ S_{n1} & \dots & S_{nm} \end{pmatrix} \tag{1}$$

The general term S_{ij} is the ith measurement on the jth snapshot. We then define the matrix Φ, whose general term is:

$$\Phi_{ij} = S_{ij} - \bar{S}_i \tag{2}$$

where $\bar{S}$ is the average snapshot vector. The correlation matrix $\mathbf{C}$ can then be obtained:

$$\mathbf{C} = \mathbf{\Phi}\mathbf{\Phi}^T \tag{3}$$

$\mathbf{C}$ is a square matrix of dimension n. Because the number of measurements per snapshot is usually high, the correlation matrix is large.

3 Extraction of the features of the random field

POD allows one to decompose the random field on a basis made of the eigenvectors of the correlation matrix. POD is similar, in concept, to the Karhunen–Loeve (KL) decomposition (Ghanem and Spanos 1991). It has to be emphasized that the main difference between the two decompositions comes from the fact that KL includes a probabilistic aspect in the decomposition, whereas POD does not. That is:

$$S_i = \bar{S} + \sum_{j=1}^{j=m} \alpha_{ij} V_j \tag{4}$$

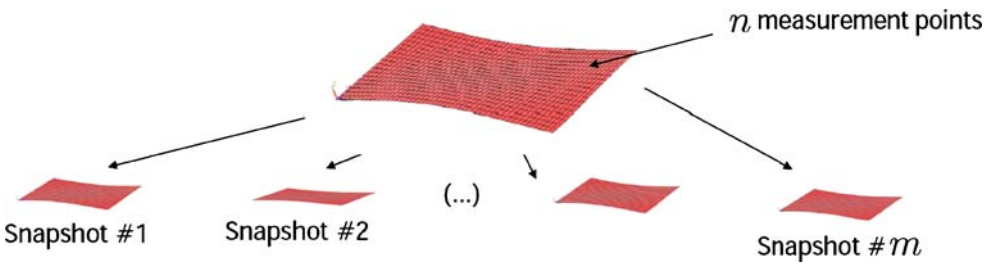

Fig. 1 Example of m snapshots with n measurement points

S_i is the measurement vector of the ith snapshot. V_j is the jth eigenvector of the correlation matrix, and α_{ij} are coefficients. The eigenvector basis being orthogonal, the general expression of the coefficients is obtained by projection:

$$\alpha_{ij} = \frac{\Phi_i . V_j}{\|V_j\|^2} \tag{5}$$

where $\Phi_i = S_i - \bar{S}$ is the ith centered snapshot and $\|.\|$ is the euclidean norm. For normalized eigenvectors ($\|V_j\| = 1$), the coefficients are:

$$\alpha_{ij} = \Phi_i . V_j \tag{6}$$

Due to the high dimensionality of the correlation matrix, finding the eigenvectors might be intractable. However, it can easily be shown that (Turk and Pentland 1991):

$$V_i = \mathbf{\Phi} V_i' \tag{7}$$

where V_i' is an eigenvector of $\mathbf{C}'$ defined as $\mathbf{C}' = \mathbf{\Phi}^T \mathbf{\Phi}$.

This square matrix is of dimension m. Because m is the number of snapshots, which is typically small compared to the number of measurements n, the extraction of eigenvectors becomes straightforward. Once these vectors are obtained, (7) is used to find the eigenvectors of the correlation matrix $\mathbf{C}$.

The inspection of the m eigenvalues λ_i of $\mathbf{C}$ provides an insight into the "importance" of the features (i.e., eigenvectors). The lowest eigenvalues correspond to the least important features. Therefore, by ranking the m eigenvalues, one can select the ms most important features. This ranking is typically performed by inspecting the ratio ρ_i of the ith eigenvalue to the sum of all eigenvalues (Bui-Thanh et al. 2003):

$$\rho_i = \frac{\lambda_i}{\sum_{j=1}^{m} \lambda_j} \tag{8}$$

The expansion containing less than m eigenvectors can only *reconstruct* approximately the original snapshots. The final expression of the expansion reads:

$$\tilde{\Phi}_i = \sum_{j=1}^{j=ms} \alpha_{ij} V_j \tag{9}$$

where $\tilde{\Phi}_i$ is the approximate reconstruction of the ith centered snapshot. The mean square error due to the truncation of the expansion is given by the following relation (Ghanem and Spanos 1991):

$$\epsilon^2 = \frac{1}{m} \sum_{j=1}^{j=m} (S_j - \tilde{S}_j)^2 = \sum_{j=ms+1}^{m} \lambda_j \tag{10}$$

Note that the upper index of the sum is m and not n because the eigenvalues with indices ranging from $(m+1)$ to n are equal to zero ($\mathbf{C}'$ and $\mathbf{C}$ have the same rank).

4 Perturbation of the random field

In the previous section, it was shown that it is possible to describe the features of a random field with m observations through POD. If one wants to investigate the effect of uncertainties for design purposes, a discrete set of observations might not be sufficient to describe the potential "configurations" of the random field. In this article, we attempt to describe the randomness of the field based on varying combinations of the extracted features, which are fixed.

The idea is to generate a "continuous" random field (as opposed to a fixed set of observations) by introducing weight functions that allows one to modify the contribution of each feature. The random field $\tilde{S}$ is obtained as follows:

$$\tilde{S} = \bar{S} + \sum_{j=1}^{j=ms} N_j \alpha_{1j} V_j \tag{11}$$

N_j is the weight functions. Note that in (11), α_{1j} is used (i.e., the coefficients that are used for snapshot S_1), but this choice is arbitrary and does not remove any generality to the approach.

In this paper, Lagrange polynomials are used, and the weight functions are the traditional shape functions found in finite element approximations:

$$N_j = \prod_{j=1, i \neq j}^{ms} \frac{\eta - \eta_j}{\eta_i - \eta_j} \tag{12}$$

When two features are used with $\eta_1 = -1$ and $\eta_2 = 1$, the functions are:

$$N_1 = \frac{1-\eta}{2} \quad \text{and} \quad N_2 = \frac{1+\eta}{2} \tag{13}$$

Therefore, by varying η, one can describe combinations of the features, and therefore, span more random fields. In the remaining of this paper, η will be referred to as the "weight," although the actual weights are a function of η. Note that, although the interpolation could use several weights, this study is restricted to one.

5 Probabilistic optimization

In the context of reliability assessment or probabilistic optimization, the weight can be used as a random parameter whose properties are not modifiable during the

optimization. The probabilistic distribution of the parameter is arbitrary, but a uniform distribution makes the contribution of each feature equally probable. The probabilistic optimization problem reads:

$$\begin{aligned} \max_{x} \quad & f(x,\eta) \\ s.t. \quad & g_R(x,\eta) \le 0 \\ & g_D(x,\eta=0) \le 0 \end{aligned} \tag{14}$$

g_R and g_D represent probabilistic and deterministic constraints, respectively. Note that the deterministic constraints are evaluated at $\eta = 0$. The objective function can be deterministic or probabilistic.

6 Examples

6.1 Buckling of a plate

This section provides an example of feature extraction of a random field. The problem presented is a plate that should be perfectly planar. However, geometric imperfections creating out-of-plane deformations are present and form a random field. The plate has dimensions $a = 1$ m, $b = 0.5$ m, and a thickness $t = 1$ cm. h represents the out-of-plane coordinate, which is zero if the plate is perfectly planar. In the absence of a real-world process at the origin of a random field, the "snapshots" have to be created from an artificial field. It is assumed that the random field h is of the form:

$$h(x,y) = \frac{1}{10}\sin(K \times \Pi \times \frac{x}{a})\cos(L \times \Pi \times \frac{y}{b}) \tag{15}$$

The snapshots are created by randomly selecting values of K and L. K and L are normally distributed in an interval ranging from 0.9 to 1.1. Both the mean and the standard deviation are equal to one. As an example, if 500 snapshots are created, the three first ratios of eigenvalues as defined in (8) are 0.6151, 0.3742, and 0.0070. The remaining ratios can be considered equal to zero. Clearly, the ratios indicate that only the two first features are important. The two eigenvectors V_1 and V_2 are depicted in Fig. 2.

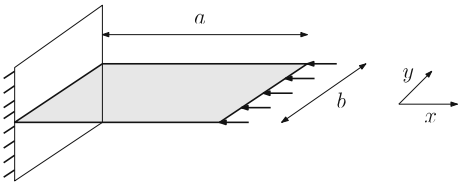

Fig. 3 Plate subjected to an in-plane load for the study of buckling load with respect to variations of the random field

In the case of two features, the random field is described as:

$$h(\eta) = \frac{1-\eta}{2}\alpha_{11}V_1 + \frac{1+\eta}{2}\alpha_{12}V_2 \tag{16}$$

To study the influence of the random field, the linear buckling of the plate is studied. The plate is clamped on one side and is subjected to an in-plane unit load as depicted in Fig. 3.

Without the shape change introduced by the random field, the critical load factor is 1,119.1. When the random field is introduced, the ratio of critical load to the critical load without the random field (nominal load factor) is plotted with respect to variations of η (Fig. 4). This is an academic example, and the scale of the perturbation as given by (15) is an exaggeration of a real random field. However, this helps to clearly show the effect of the various features on the load factor.

The behavior depicted in Fig. 4 allows one to show the influence of the first feature for a weight η in the neighborhood of -1.0 and the second feature for η close to $+1.0$. Note that, for this amplitude of random imperfections, the ratio of eigenvalues consistently shows that only two features are needed, independently of the number of snapshots. However, if larger amplitude is used, then a larger number of features might be required. There might also be large variations of the

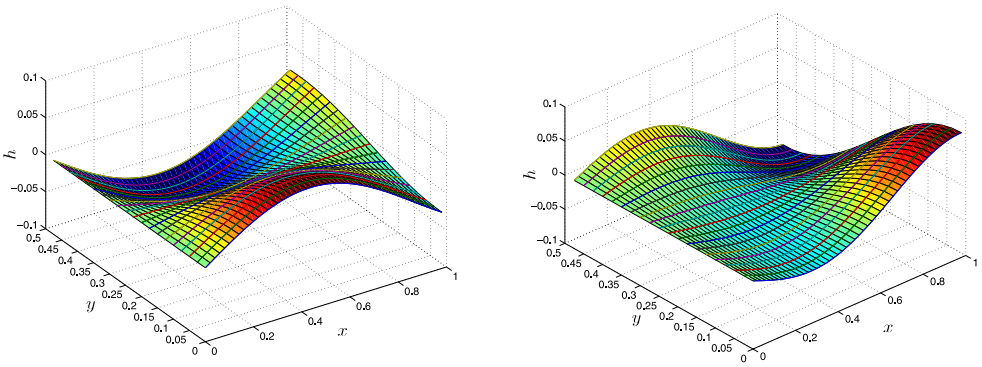

Fig. 2 First and second eigenvectors V_1 and V_2 of the random field correlation matrix

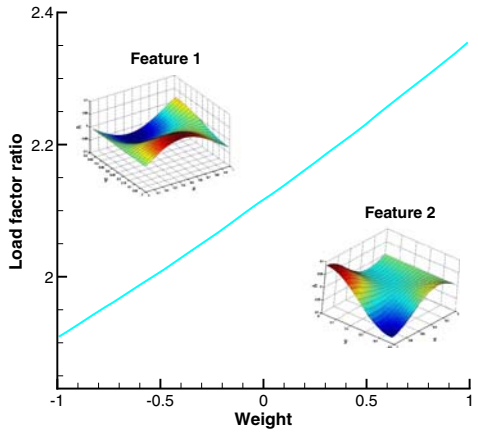

Fig. 4 Ratio of buckling load factor to nominal load factor with respect to weight. Linear buckling of a plate. Random field approximation based on two eigenvectors

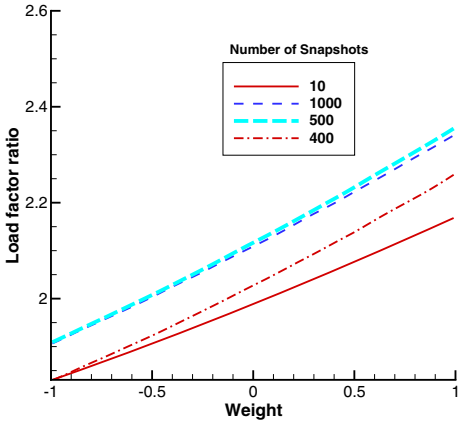

Fig. 6 Ratio of buckling load factor to nominal load factor with respect to weight. Results for different number of snapshots

ratios with respect to the number of samples. Nevertheless, in general, imperfections are likely to be of small amplitude.

6.2 Influence of the number of snapshots

This section examines the influence of the number of snapshots on the ratio ρ_i (5) for the plate problem. Figure 5 depicts the evolution of the ratios for the first and second eigenvalues with respect to the number of snapshots.

From Fig. 5, it is quite clear that, after approximately 50 snapshots, the relative importance of the two first features is nearly constant. The ratios for the first and second features are about 60 and 40%.

However, it is also important to check how the number of snapshots affects the response of the system. That is, the variations of the first critical load are studied with respect to the number of snapshots. Figure 6 depicts the variation of the ratio of the first critical load to the nominal load factor.

Beyond a certain number of snapshots, the variation of the response diminishes. From this study, it appears that the system's response does not vary much beyond 500 samples. Note that, for this academic problem, the amplitude of the geometric imperfections is high. For real-world imperfections, the variations triggered by different number of snapshots would clearly be much smaller.

6.3 Tube impacting a rigid wall

The previous methodology is extended to the probabilistic optimization of a tube impacting a rigid wall (Fig. 7). Four rear masses of total mass 60 kg are used. The velocity of the tube before impact is 10 m/s. The tube is $a = 0.6$ m long and has a square section of

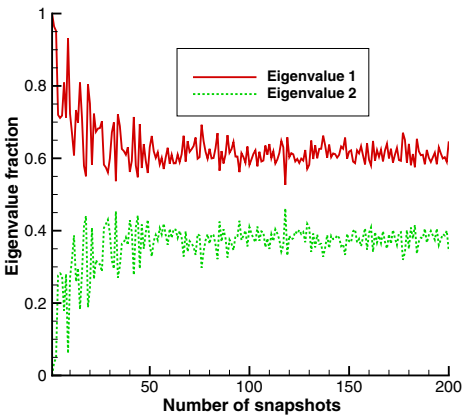

Fig. 5 Ratio of the first and second eigenvalues to the total sum of eigenvalues with respect to the number of snapshots

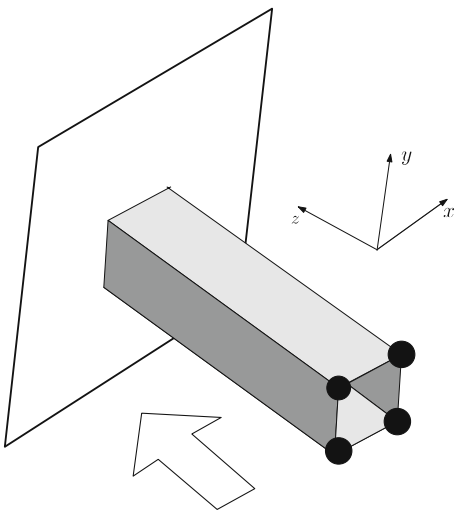

Fig. 7 Tube with square section and rear masses impacting a rigid wall

Fig. 8 Random field snapshot generated for one face of the tube (*left*). Application to all four faces of the tube (*right*)

side $b = 5.0$ cm. A thickness of 2.5 mm, considered constant over the whole tube, is used. The analysis is performed with the explicit code LS-Dyna with ANSYS as a pre- and postprocessor. This is a nonlinear transient dynamic problem that exhibits a very acute sensitivity to imperfections.

Similar to the plate's case, a random field modifies the planarity of the tube's sides. The same random field is applied to the four sides of the tube. In the absence of experimental results, an arbitrary random field is generated using the following equation:

$$h(x_L, z_L) = \frac{W}{100} \sin(K \times \Pi \times \frac{x_L}{b}) \cos(L \times \Pi \times \frac{z_L}{a}) \tag{17}$$

x_L and z_L are the local coordinates on each of the four faces. W is a scalar that globally modifies the amplitude of the random field. W takes values between 1.0 and 2.0. K has a fixed value of 3.0, and L is chosen randomly between 1.0 and 3.0. An example of snapshot for one face of the tube is given in Fig. 8 along with the aspect of the whole tube. The deformation on the snapshot has been exaggerated for visibility. Note that the field is created so that the positions of the nodes on the corner sides of the tube are not modified. From (17), 100 snapshots were created. Based on the eigenvalues of the correlation matrix, two features, corresponding to the two first eigenvectors, were selected. Table 1 provides the eigenvalues in decreasing order as well as their ratios to the sum of eigenvalues, thus, showing the rationale for only choosing the two first features.

In this problem, the goal is to maximize the probability of having a given energy absorption. It is assumed that the changes in the behavior of the tube are solely due to the random field described above. Structural fuses are used to modify the design of the tube and control its behavior. In a previous paper by the author (Missoum 2007), structural fuses were used to enforce the crushing of a similar tube impacting a rigid wall. However, this had been done for uncertainties in the form of a random thickness independent of the position on the tube.

The two fuses are in the form of square openings (Fig. 9) whose center positions are x_1 and x_2. The positions can vary from 0.1 to 0.5 m. They are symmetrically positioned on each side of the tube. The height and width of the openings is 2.5 cm. More details about structural fuses can be found in Missoum (2007). Defining ER as the energy ratio (ratio of strain energy to total energy), the optimization problem reads

$$\begin{aligned} \max_{x_1,x_2} \quad & Prob\,(ER(x_1, x_2, \eta) \geq 0.5) \\ s.t. \quad & 0.1 \leq x_1 \leq 0.5 \\ & 0.1 \leq x_2 \leq 0.5 \end{aligned} \tag{18}$$

In this paper, the coefficient η that is used to "mix" the two features is considered as a random variable with uniform probabilistic distribution (Fig. 10).

To find the optimal fuse locations, a simple design of experiments is carried out on the fuse positions x_1 and x_2, with five levels each. Although this leads to 25 cases, only 15 cases need to be evaluated due to the symmetry of the fuse positions. To assess the effect of uncertainties on the response, η is sampled uniformly ($n = 16$ times) for each fuse configuration (Fig. 11). Note that, at this stage, even if the probabilistic distributions of η were not uniform, the sampling would still be uniform. The actual probabilistic distribution is only considered for the calculation of the probabilities. For each fuse configuration, two groups of points are created by seg-

Table 1 Eigenvalues (in decreasing order) corresponding to the features of the random field

	Eigenvalue λ_i	Ratio ρ_i (%)
Feature 1	2,579.4	63.1
Feature 2	1,224.0	29.9
Feature 3	280.9	6.9
Feature 4	3.3	0.1
Features 5–8	0.0	0.0

The ratio of the eigenvalues to the sum of eigenvalues shows the importance of the first two features.

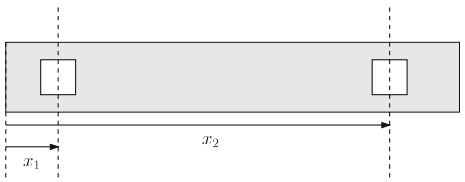

Fig. 9 Tube with two fuses located at x_{1} and x_{2}

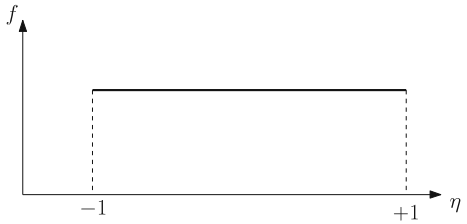

Fig. 10 Uniform probabilistic distribution for η used to weigh the contributions of the two random field's features. Tube impacting a rigid wall

regating cases with an energy ratio above and below 50%. Based on this decomposition into two groups A (energy ratio above 0.5) and B, the probability P_S of having a ratio above 0.5 can be calculated. For a one-dimensional problem, as described in Missoum (2007), this is done in the following way: let $\Delta\eta$ be the constant interval between two η values. Each point in group A is defined by the response value R_A and the associated η_A. The union of all the intervals of width $\Delta\eta$ centered around η_A forms "feasible" sub-regions, Ω_i. Figure 12 shows an example with two sub-regions.

Figures 13 and 14 show the energy ratios with respect to η for two fuse configurations. The values of all the energy ratios and probabilities for the 15 fuse configurations are presented in Table 2.

In Missoum (2007), the probability was approximated using a radial basis network to perform a reliability-based optimization. However, in the present problem, the maximum probability can be obtained by inspection: A probability of 0.84 is obtained for fuse locations of $x_1 = 0.2$ m and $x_2 = 0.2$ m. Therefore, one fuse at position 0.2 m is needed.

6.4 Discussion

In this study, arbitrary random fields were created. Due to their rather simple form, a reduced number of features was needed. However, for real-world

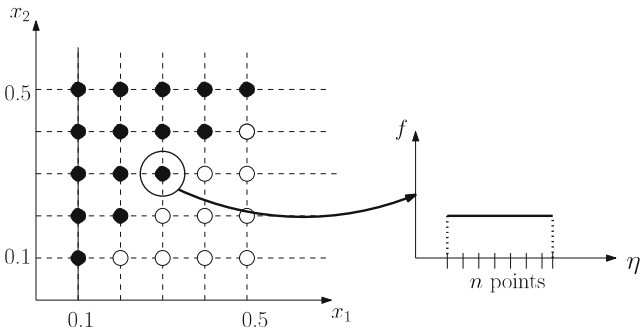

Fig. 11 Design of experiments with respect to fuse positions x_1 and x_2 and η. Uniform sampling of η with $n = 16$ samples. The *empty circles* show the cases that could be obtained by symmetry

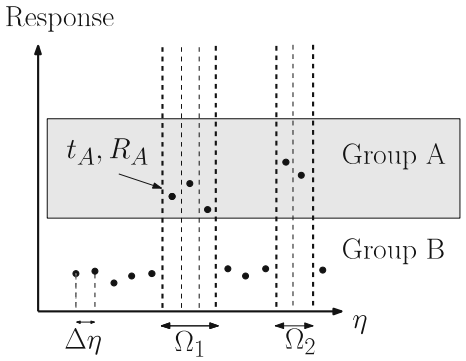

Fig. 12 Based on two groups A and B and an interval $\Delta\eta$, definition of sub-regions, Ω_i, for the calculation of the probability P_S. Example of point with coordinates $(\eta_\mathrm{A}, R_\mathrm{A})$ belonging to cluster A

applications, more features (i.e., eigenvectors) might be required. Assuming the availability of the appropriate number of snapshots, the features necessary to accurately describe the field can be obtained. Note that the methodology presented in this paper makes the feature extraction realistic even if the number of measurement points for each snapshot is extremely high (thousands or more).

To improve the proposed methodology, several points need to be addressed in future developments:

- The proposed scheme interpolates the features. Other variables modifying the amplitude of the random field could be used in the probabilistic optimization. This would allow a more conservative description of the field and minimize the influence of the error due to the use of a reduced basis of features or due to the lack of experimental data.
- The distribution for the weight was assumed uniform in the test examples. This means all the features have the same probability of occurrence. For real-world examples, the actual probabilistic density function can be gauged using the snapshots.

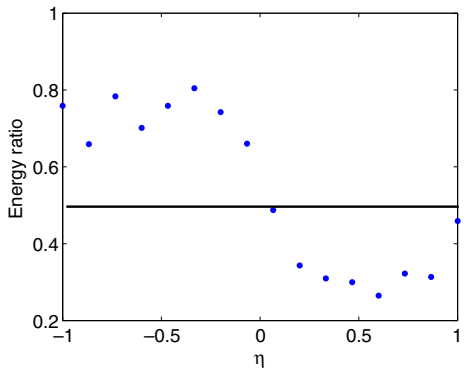

Fig. 13 Energy ratio with respect to the weight η for fuse positions $x_1 = 0.1$ m and $x_2 = 0.1$ m. The *thick horizontal line* represents the 50% energy ratio threshold

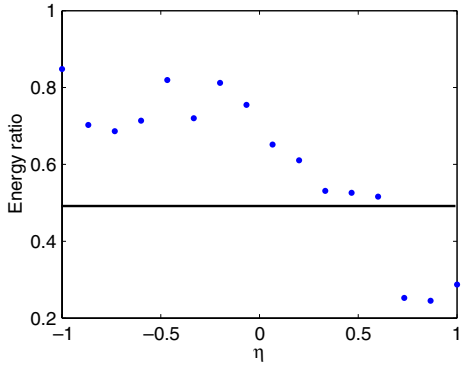

Fig. 14 Energy ratio with respect to the weight η for fuse positions $x_1 = 0.2$ m and $x_2 = 0.2$ m. The *thick horizontal line* represents the 50% energy ratio threshold

For instance, the total number of snapshots can be divided into various sets wherein the dominance of each feature is assessed. This would allow to calculate the probabilistic distribution for each feature.

- In this paper, the examples described used one weight. When multiple "weights" are used, the methodology to calculate the probabilities needs to be modified. That is, either Monte Carlo simulations can be used or the boundaries of the subregions as described in Section 6.3 can be found analytically (Harrison et al. 2006).
- The number of samples for the weights (16) might seem quite high. However, this number was used as the first approach. A smaller sample size could be used by approximating the energy ratios.

Table 2 Probability of having an energy ratio above 0.5 for the 15 cases of fuse locations

Fuse locations (m)	P_S
$x_1 = 0.1$ $x_2 = 0.1$	0.50
$x_1 = 0.2$ $x_2 = 0.1$	0.16
$x_1 = 0.2$ $x_2 = 0.2$	0.84
$x_1 = 0.3$ $x_2 = 0.1$	0.10
$x_1 = 0.3$ $x_2 = 0.2$	0.0
$x_1 = 0.3$ $x_2 = 0.3$	0.27
$x_1 = 0.4$ $x_2 = 0.1$	0.30
$x_1 = 0.4$ $x_2 = 0.2$	0.43
$x_1 = 0.4$ $x_2 = 0.3$	0.03
$x_1 = 0.4$ $x_2 = 0.4$	0.70
$x_1 = 0.5$ $x_2 = 0.1$	0.10
$x_1 = 0.5$ $x_2 = 0.2$	0.37
$x_1 = 0.5$ $x_2 = 0.3$	0.03
$x_1 = 0.5$ $x_2 = 0.4$	0.57
$x_1 = 0.5$ $x_2 = 0.5$	0.60

7 Conclusion

A methodology to handle random fields in the context of probabilistic optimization was presented. The approach uses POD, so that the field can be described through a handful of features identified from observations. The random field is then described as a varying combination of weighted features. Therefore, it is possible to perform probabilistic optimization by sampling various values of the weights. The approach is applied to the probabilistic optimization of a tube impacting a rigid wall. Other approaches to generate a random field using different relations between the features are currently being investigated.

References

Adams BA, Eldred MS, Wittwer JW (2006) Reliability-based design optimization for shape design of compliant micro-electro-mechanical systems. In: 11th symposium AIAA/ISSMO on multidisciplinary analysis and optimization, Portsmouth, Virginia

Bui-Thanh T, Damodaran M, Willcox K (2003) Proper orthogonal decomposition extensions for parametric applications in transonic aerodynamics. In: 21st AIAA applied aerodynamics conference, Orlando Florida, Orlando, Florida

Ghanem R, Spanos PD (1991) Stochastic finite elements: a spectral approach. Springer, New York

Haldar A, Mahadevan S (2000) Probability, reliability, and statistical methods in engineering design. Wiley, New York

Harrison A, Missoum S, Martinez JP (2006) Design space decomposition using support vector machines for reliability-based design optimization. In: 11th symposium AIAA/ISSMO on multidisciplinary analysis and optimization, Portsmouth, Virginia

Kharmanda G, Mohamed A, Lemaire M (2002) Efficient reliability-based design optimization using a hybrid space with application to finite element analysis. Struct Multidisc Optim 24:233–245

Melchers R (1999) Structural reliability analysis and prediction. Wiley, New York

Missoum S (2007) Controlling structural impact failure modes in the presence of uncertainty. Struct Multidisc Optim (in press). doi: 10.1007/s00158-007-0100-z

Oliveiraa DA, Michael A, Worswicka J, Grantaba R, Williams B, Mayerb R (2006) Effect of forming process variables on the crashworthiness of aluminum alloy tubes. Int J Impact Eng 32:826–846

Trosset MW, Alexandrov NM, Watson LT (2003) New methods for robust design using computer experiments. In: Proceedings of the Section on Physical and Engineering Sciences, American Statistical Association

Turk M, Pentland A (1991) Eigenfaces for recognition. J Cogn Neurosci 3(1):71–86

Youn BD, Choi KK (2004) Selecting probabilistic approaches for reliability-based design optimization. AIAA J 42(1): 124–131